Supporting Information for "Southern Ocean calcification controls on the global distribution of alkalinity"

K. M. Krumhardt[1], M. C. Long[1], K. Lindsay[1], M. Levy[1]

[1]Climate and Global Dynamics, National Center for Atmospheric Research, Boulder, Colorado, U.S.A.

Contents of this file

1. Figures S1 to S10

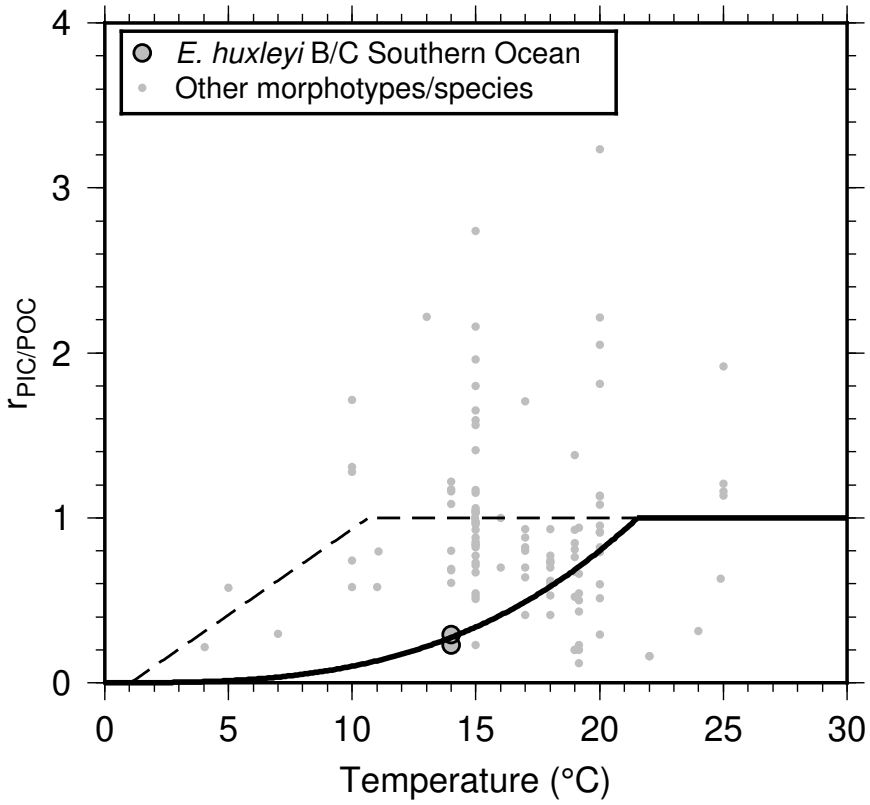

Figure S1. Refined particulate inorganic carbon (PIC) to particulate organic carbon (POC) production ratio in coccolithophore growth in CESM2 with coccolithophores. The new relationship is shown by the solid black line, while the relationship used previously (Krumhardt et al., 2019) is shown by the dashed line. Data points from experiments with the Southern Ocean *Emiliania huxleyi* morphotype are enlarged and outlined with black circles.

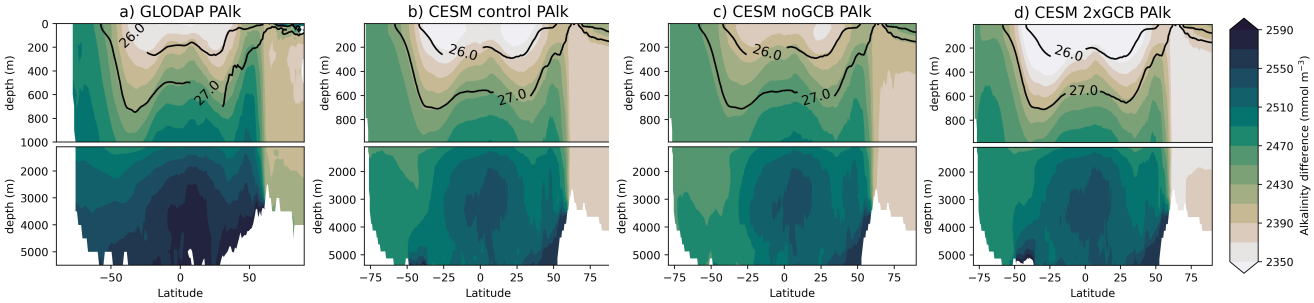

Figure S2. Zonal mean salinity-normalized potential alkalinity (PAlk) from (a) observations (GLODAP v2), (b) CESM control, (c) CESM noGCB experiment, and (d) CESM 2xGCB experiment. The CESM control and experiments are averaged over the last 62 years of our model simulation.

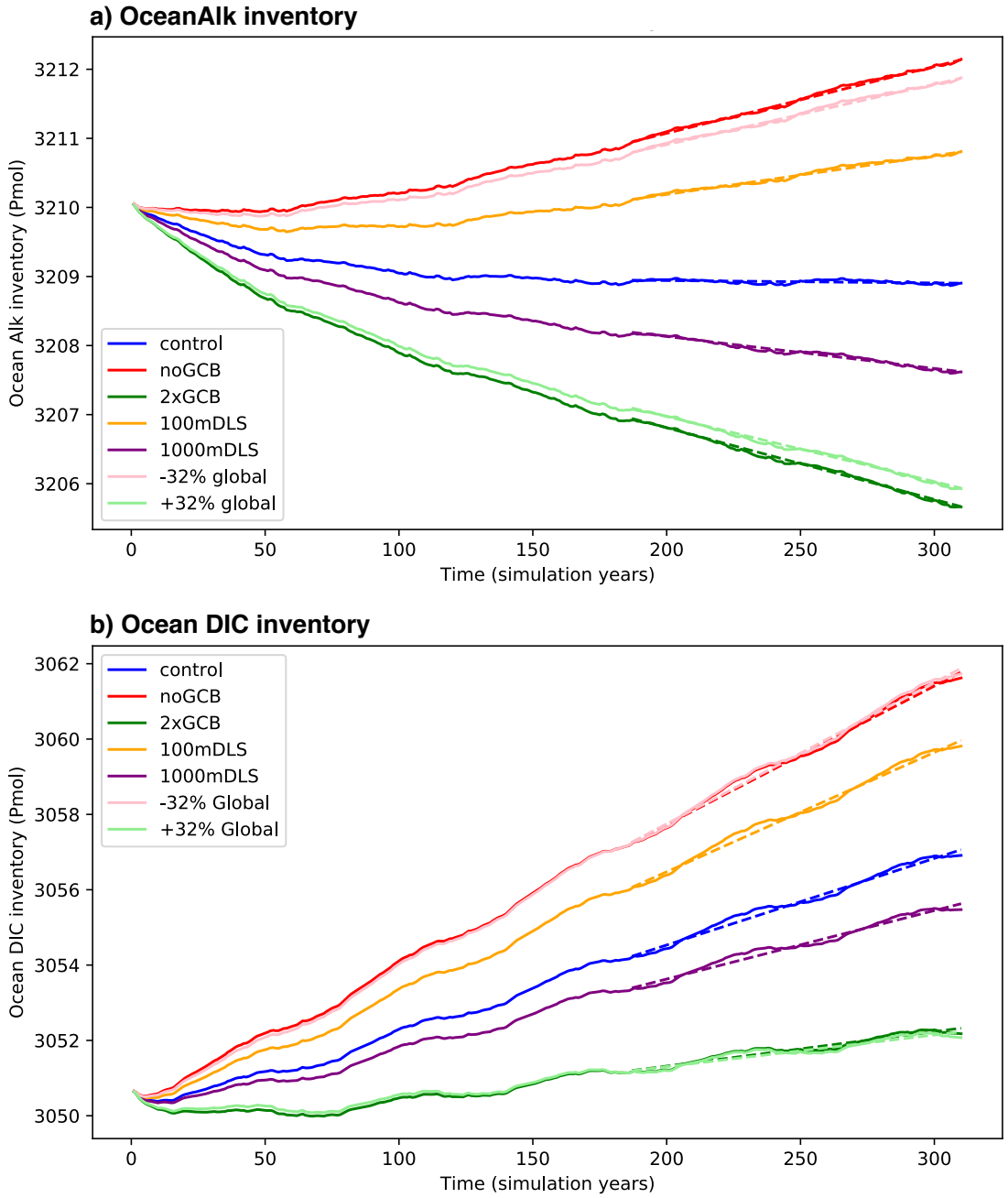

Figure S3. Ocean Alkalinity (Alk; panel a) and dissolved inorganic carbon (DIC; panel b) inventory time-series over the course of each experiment and the control. Least-squares regression lines were computed over the last two interannual forcing cycles (124 years), shown here in dashed lines. The slopes of these lines (Alk and DIC accumulation rates) are reported in Table 1.

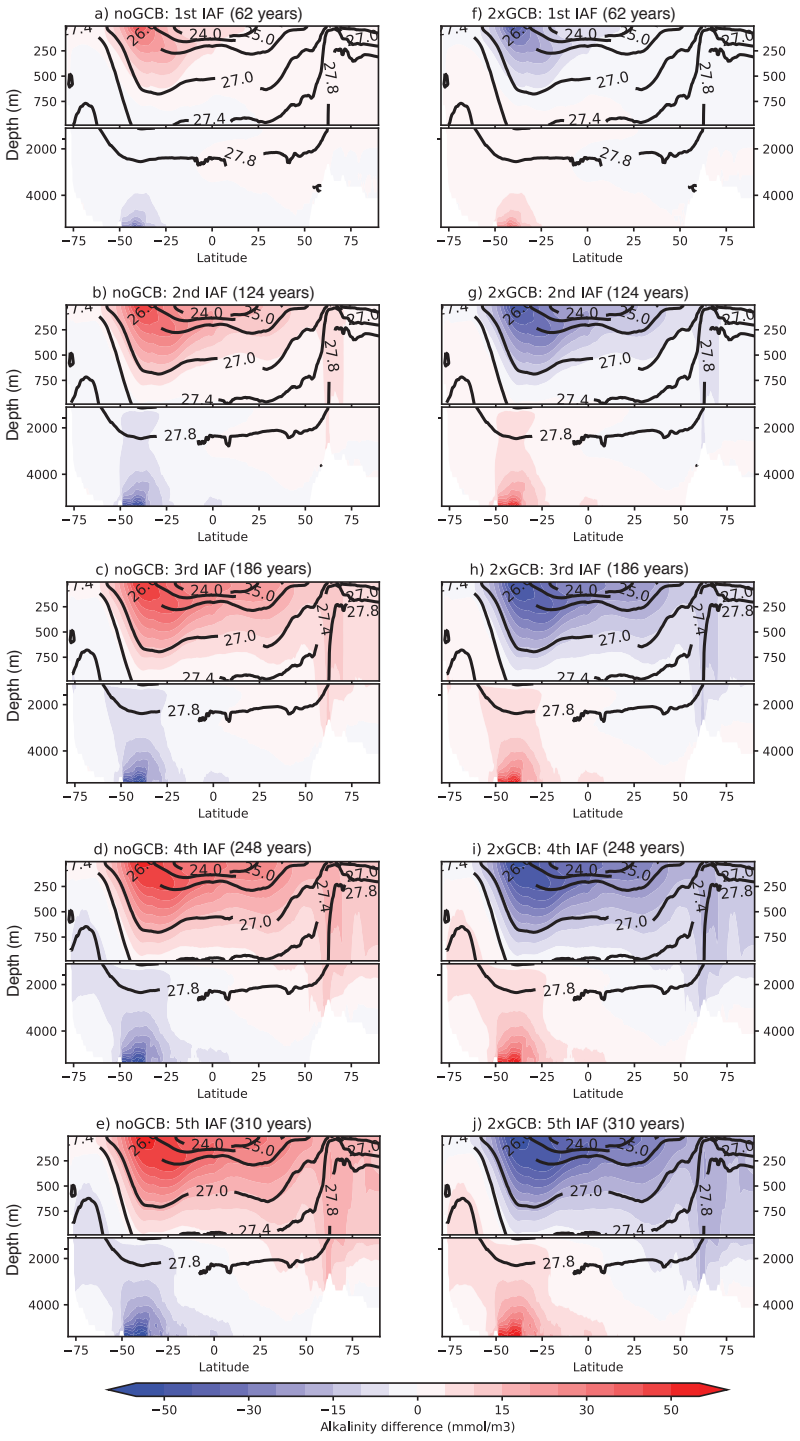

Figure S4. Zonal global mean differences (experiment - control) in alkalinity between the control and the noGBC experiment (panels a-e) and the 2xGBC experiment (panels f-j). Each row is representative of a mean zonal difference for each interannual forcing (IAF) cycle (62 years/cycle), with the first IAF cycle on the top row and the fifth on the bottom. Isopycnal layers in σ_θ coordinates are shown by contour lines. The final year of each IAF cycle is indicated for each plot.

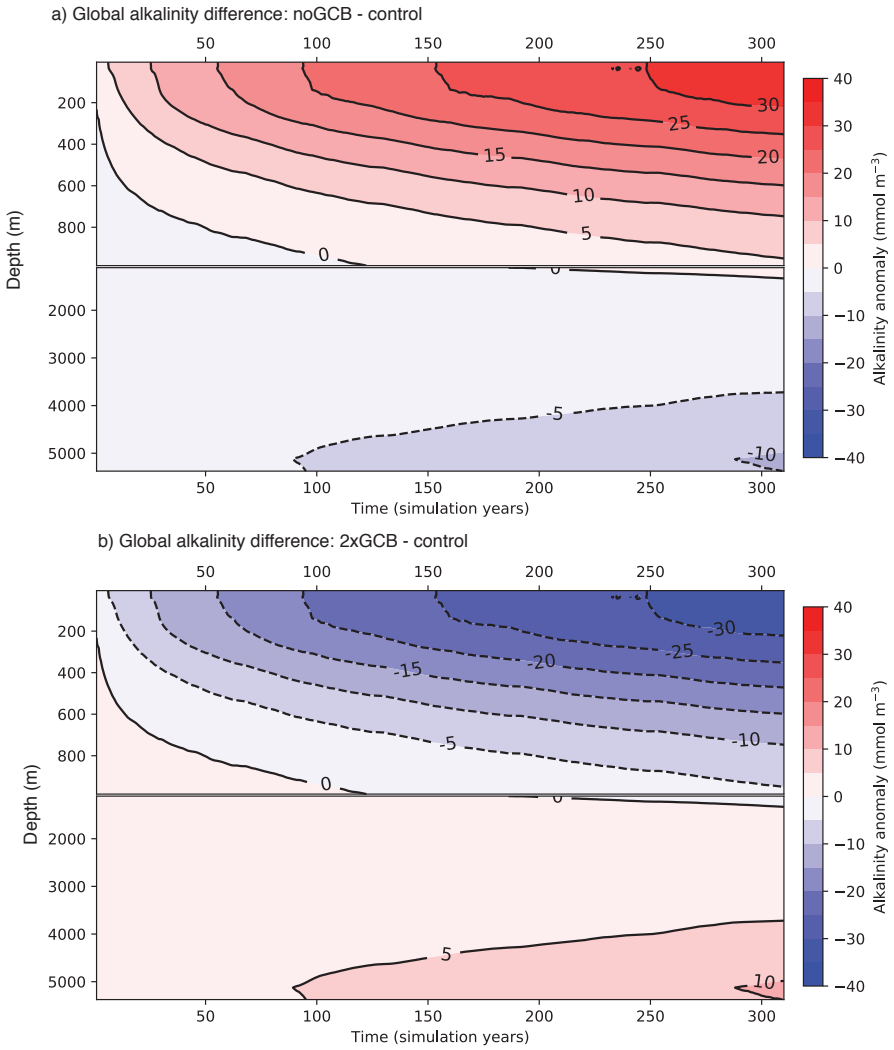

Figure S5. Global mean Hovmöller diagrams of alkalinity anomalies (experiment - control) for the noGCB (a) and 2xGCB (b) experiments. Panels show alkalinity differences from the control in a depth versus time field for our 310-year CESM integrations. Note the explanded top 1000m depth axis.

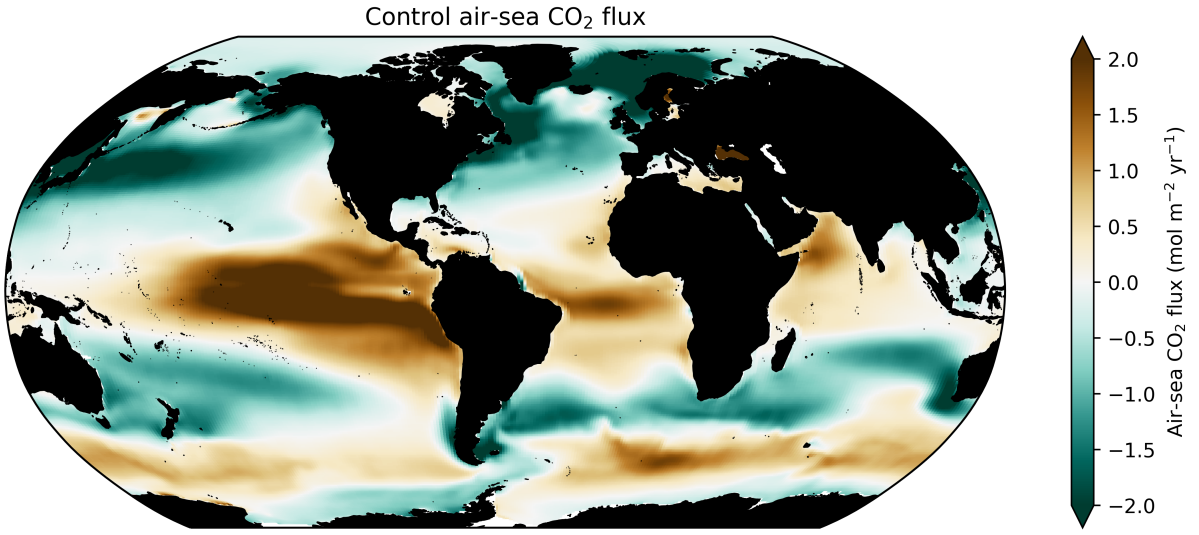

Figure S6. Air-sea CO_2 flux from the control simulation in mmol m^{-2} yr-1 (mean over the last IAF cycle, last 62 years of the simulation).

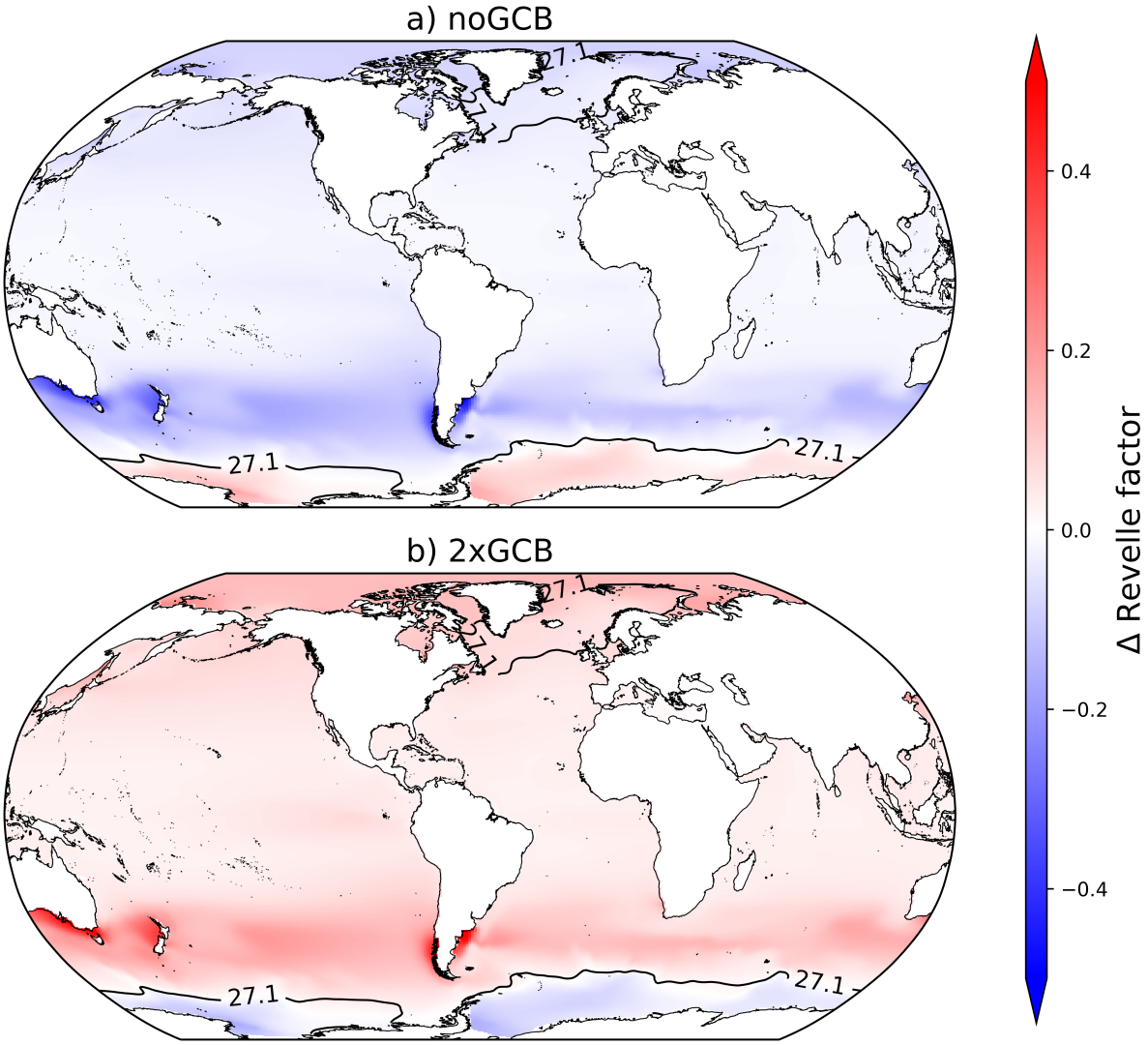

Figure S7. Changes (experiment - control) in the Revelle factor relative to the control for the noGCB experiment (a) and the 2xGCB experiment (b) (mean over the last IAF cycle, last 62 years of the simulation).

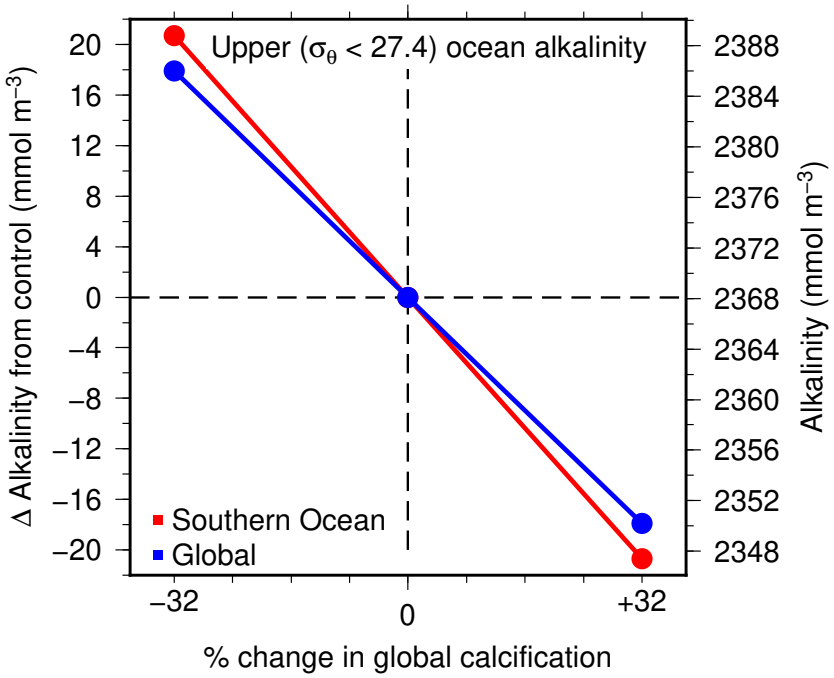

Figure S8. Mean alkalinity in the upper ocean ($\sigma_\theta < 27.4$) as a function of globally integrated changes in calcification. The red line shows the change in alkalinity when the calcification perturbation is isolated in the Southern Ocean (south of 30°S; noGCB and 2xGCB experiments). The blue line shows the change in alkalinity when the calcification perturbation is spread out over the entire ocean (-32Global and +32Global experiments; see Table 1 in main text).

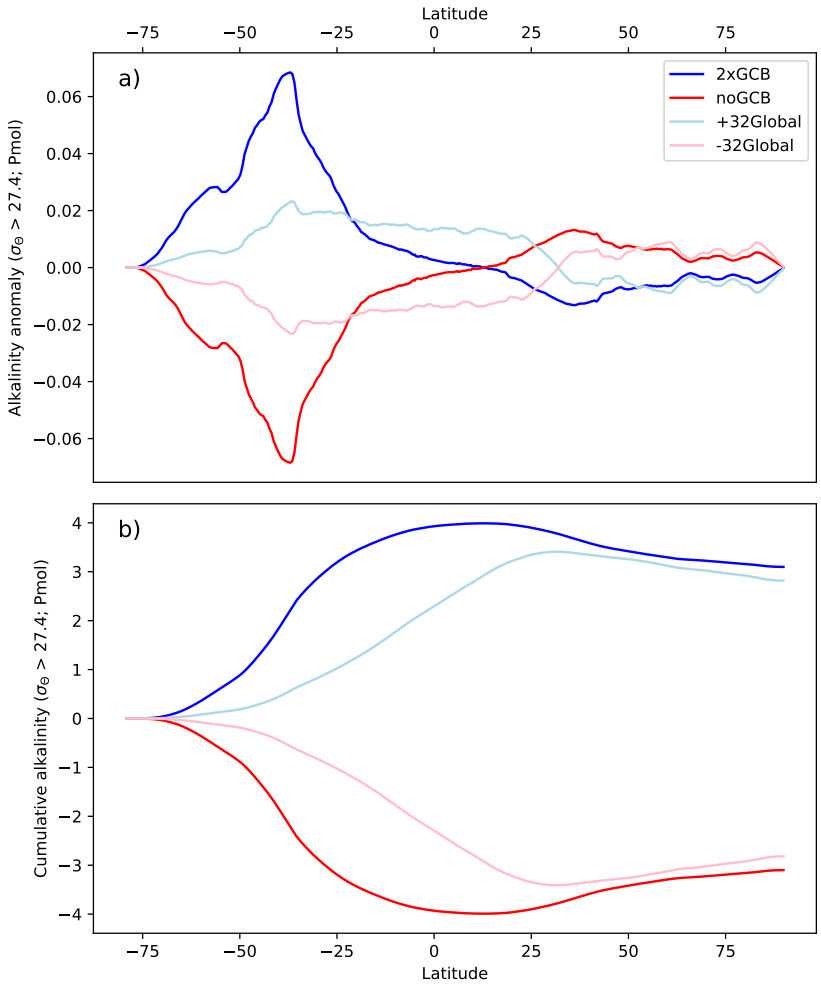

Figure S9. Deep ocean ($\sigma_\theta > 27.4$) alkalinity inventory anomaly (a) and cumulative deep ocean alkalinity inventory anomaly (b) as a function of latitude. The anomalies are with respect to the control integration (experiment - control). The large anomalies in the southern latitudes shown on panel (a) for experiments 2xGCB and noGCB represent the Southern Ocean alkalinity trap, absent in the -32Global and +32Global experiments. The cumulative alkalinity anomalies on panel (b) show how the Southern Ocean alkalinity trap affects overall deep ocean alkalinity inventories, relative to changing calcification globally.

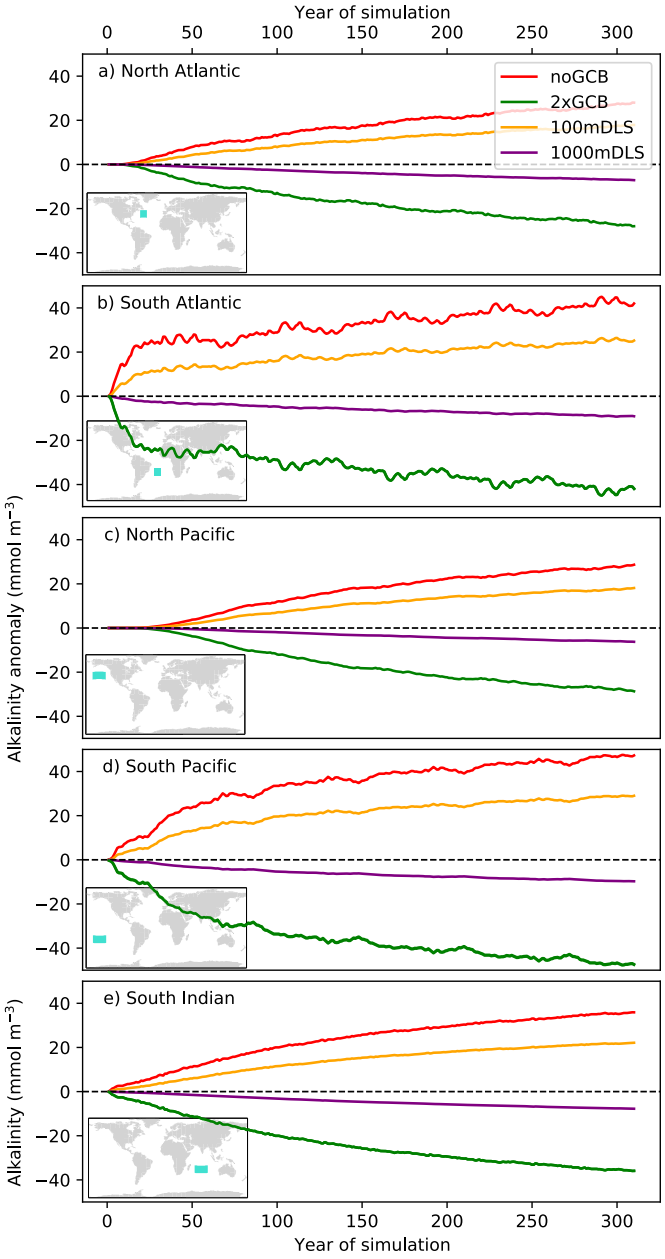

Figure S10. Timeseries of mean alkalinity anomalies in the top 150 m in each of our experiments relative to the control for five subtropical boxes in the (a) North Atlantic, (b) South Atlantic, (c) North Pacific, (d) South Pacific, and (e) South Indian. Box locations are shown by the small inset maps in each panel. One caveat to these timeseries plots is that the model flow is not spun up at the beginning of these integrations, so dynamics may not be simulated adequately to fully assess the propagation of the alkalinity anomaly signal.

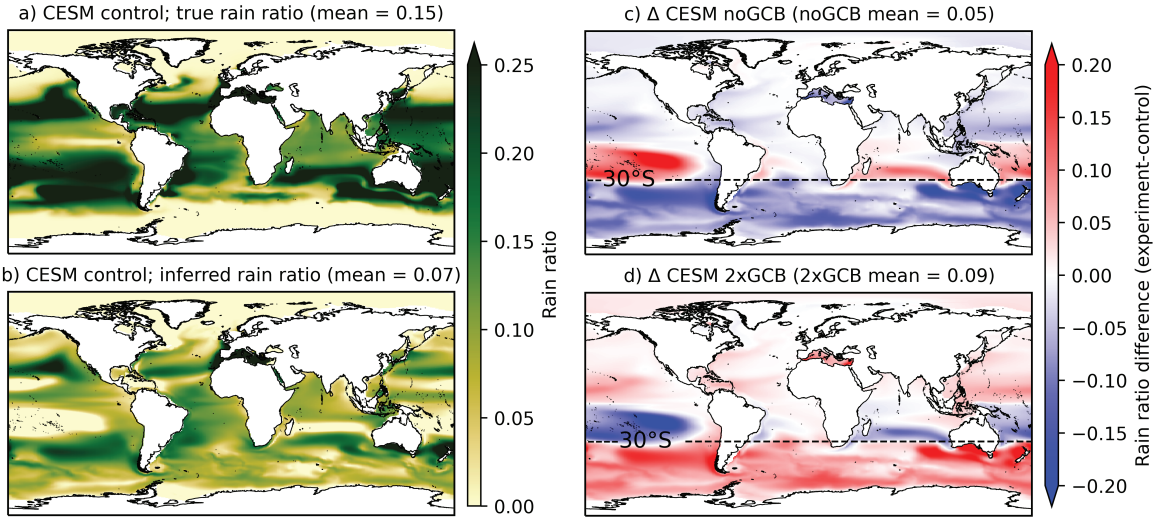

Figure S11. The true rain ratio (a) and inferred rain ratio (calculated as in Sarmiento et al., 2002) for the CESM control simulation, and changes in the inferred rain ratio for the noGCB (c) and 2xGCB (d) experiments, with reference to the control. The true rain ratio is the ratio of $CaCO_3$ flux and particulate organic carbon flux at 100 m. The inferred rain ratio is based on vertical gradients of salinity-normalized potential alkalinity and salinity-normalized nitrate (Sarmiento et al., 2002).